NUMERICAL INVESTIGATION OF THE GENERALIZED PINCH-DIFFUSION EQUATIONS IN THE EDGE PEDESTAL

JOHN-PATRICK FLOYD* and W. M. STACEY

Georgia Institute of Technology, Fusion Research Center, 770 State Street, Atlanta, Georgia 30332-0745

Received April 29, 2011
Accepted for Publication August 16, 2011

The presence of a large pinch velocity in the edge pedestal of high-confinement (H-mode) tokamak plasmas implies that particle transport in the plasma edge must be treated by a generalized pinch-diffusion theory, rather than a pure diffusion theory. An investigation of extending the numerical solution methodology of the standard diffusion theory to the solution of the generalized pinch-diffusion theory has been carried out. It is found that in the edge pedestal, where the inward pinch velocity is large in H-mode plasmas, a finer mesh spacing will be required than is necessary for similar accuracy farther inward, where the pinch velocity diminishes. An expression for the numerical error in various finite-differencing algorithms is presented.

KEYWORDS: *pinch-diffusion, edge transport, generalized diffusion equation*

I. INTRODUCTION

The high-confinement (H-mode) edge pedestal, a steep-gradient region just inside the separatrix over which the plasma pressure increases rapidly, is an area of intense research interest[1] because of experimental[2–4] and theoretical[5,6] evidence indicating that the performance of future tokamaks may be strongly linked to the values of the temperatures and densities at the top of the pedestal. An important aspect of these studies is the development of predictive and interpretive capabilities for accurate modeling of ion transport in the edge. Currently, these computational efforts center around 1.5-dimensional (1.5-D) and 2-dimensional (2-D) codes [e.g., ONE-TWO (Ref. 7), GTEDGE (Ref. 8), ASTRA (Ref. 9), SOLPS (Ref. 10), and UEDGE (Refs. 11 and 12)], which solve the plasma fluid balance equations for particle, momentum, and energy balance in one or two geometric dimensions, utilizing 1-dimensional (1-D) or 2-D calculations of recycling neutral density.

The plasma particle transport analysis in these types of codes is often based on a purely diffusive model of particle transport, $\Gamma = -D\nabla n$, although some codes have a capability to also represent convective transport. Here, D is the diffusion coefficient, n is the particle density, and Γ is the particle flux. The use of diffusion theory methodology to interpret diffusion coefficients from experimental density profiles often produces unrealistically small values.[13] This result prompted an investigation into the form of the particle transport flux required by particle and momentum balance,[14] which determined that momentum balance required the ion radial transport flux to satisfy a pinch-diffusion relationship, $\Gamma = -D\nabla n + nV_r^{pinch}$, and not a purely diffusive relationship, $\Gamma = -D\nabla n$. Here, V_r^{pinch} is the radial particle pinch velocity, which is produced by the $V \times B$ force, the radial electric field, and other forces.[14] These investigations[14] also found that the convective term (which includes the particle pinch velocity) in the pinch-diffusion formalism nearly balances the diffusion term.

Substitution of the pinch-diffusion relation into the continuity equation leads to a generalized diffusion equation including diffusive, second-derivative terms and convective, first-derivative terms incorporating the pinch velocity.[15] This raises the question of modifying the existing codes mentioned above, most of which are based on a pure diffusion relation for the radial particle flux, to solve the generalized diffusion equations for the

*E-mail: johnp.floyd@gatech.edu

situation in which the nondiffusive "pinch" term is comparable to the diffusive term.

The purpose of this paper is to report on a first numerical investigation into the adaptation and extension of solution methodology that has been developed for the diffusion equation to solve the generalized diffusion equation in the situation when the convective pinch term is comparable with the diffusive term. This 1-D analysis is relevant to 1.5-D codes directly and provides insight into the numerics and accuracy for 2-D codes.

II. GENERALIZED PINCH-DIFFUSION EQUATION

The idea that the centrally peaked density profiles observed in edge-fueled tokamaks are evidence of an inward particle pinch is as old as tokamak research itself,[16,17] and many researchers represent the total radial particle flux as a diffusive component plus a convective component (e.g., Ref. 18), using the pinch-diffusion relation

$$\Gamma = -D\nabla n + nV_r^{pinch} \quad . \tag{1}$$

Detailed numerical modeling,[19] recent interpretive calculations,[20] experimental observations of pedestal density[21] and electron density barrier width expansions in time between edge-localized modes[22] (ELMs) in DIII-D discharges, and 2-D modeling of edge-diagnostics-optimized Joint European Torus (JET) discharges[23] all seem to require a strong pinch term to explain. These findings motivate the present work.

II.A. The Pinch-Diffusion Relation

The pinch-diffusion relation[15] used in this work to describe edge transport was derived in response to the nonphysical diffusion coefficients inferred from some experiments with the use of pure diffusion theory. It is a common practice to determine the values of the diffusion coefficient by fitting radial density profiles with the purely diffusive model, resulting in a spatially varying diffusion coefficient profile. While such a fitting procedure has provided some insight in the past, it has on occasion led to nonphysically small values of the inferred diffusion coefficients and is now recognized as being inconsistent with momentum balance. Momentum balance requirements on the form of an edge transport model mandate that the particle flux satisfy a pinch-diffusion model.[24]

For completeness, we summarize here the development of the pinch-diffusion relation and the generalized diffusion theory.[15] Using some simplifying assumptions about the carbon ion impurity (k) distribution, the toroidal and radial momentum balance equations

$$n_j m_j[(\nu_{j,k} + \nu_{d,j})V_{\phi,j} - \nu_{j,k}V_{\phi,k}] = n_j e_j E_\phi^A + n_j e_j B_\theta V_{r,j} + M_{\phi,j} \tag{2}$$

and

$$V_{\phi,j} = \frac{1}{B_\theta}\left[E_r + V_{\theta,j}B_\phi - \frac{1}{n_j e_j}\frac{\partial p_j}{\partial r}\right] \tag{3}$$

can be rearranged to obtain[25] a pinch-diffusion relation for the main ion (j) radial particle flux:

$$\Gamma_j \equiv n_j V_{r,j} = -\frac{n_j D_j}{p_j}\frac{\partial p_j}{\partial r} + n_j V_{r,j}^{pinch} \quad , \tag{4}$$

where

subscripts j, k, e = properties of deuterium, carbon, and electrons, respectively

m = particle mass

V_ϕ = particle toroidal rotation velocity

e = particle charge

B_θ = poloidal magnetic field

B_ϕ = toroidal magnetic field

V_r = radial particle velocity

V_θ = particle poloidal rotation velocity

p = pressure ($p = nT$)

E_r = radial electric field.

The quantity $\nu_{d,j}$ is a toroidal angular momentum transfer frequency, which represents the combined effect of viscosity, inertia, atomic physics, and other "anomalous" processes. Justification for representing these toroidal momentum transfer processes in this form is discussed in Ref. 15. Also, $\nu_{j,k}$ is the collisional momentum transfer frequency between deuterium and carbon ions, which can be calculated using the measured density and temperature; E_ϕ^A is the induced toroidal electric field, a small term near the separatrix that can be determined from the measured loop voltage; and M_ϕ is the external momentum input rate, another small term in the edge that can be calculated using the neutral beam geometry and power input.

The diffusion coefficient D_j and pinch velocity $V_{r,j}^{pinch}$ terms shown in Eq. (4) are a result of the above force balance and are defined as such:

$$D_j \equiv \frac{m_j T_j \nu_{j,k}}{(e_j B_\theta)^2}\left(1 + \frac{\nu_{d,j}}{\nu_{j,k}} - \frac{e_j}{e_k}\right) \tag{5}$$

and

$$V_{r,j}^{pinch} \equiv \frac{-M_{\phi,j}}{n_j e_j B_\theta} - \frac{E_\phi^A}{B_\theta} + \frac{m_j(v_{j,k}+v_{d,j})(B_\phi V_{\theta,j}+E_r)}{e_j B_\theta^2} - \frac{m_j v_{j,k} V_{\phi,k}}{e_j B_\theta} \quad . \tag{6}$$

The quantity T is the particle temperature.

II.B. Generalized Pinch-Diffusion Equation

Equation (4) for the pinch-diffusive radial particle flux can be substituted into the time-independent particle continuity equation for ion species j,

$$\nabla \cdot \vec{\Gamma}_j \equiv \nabla \cdot n_j \vec{V}_j = S_j \quad , \tag{7}$$

where S_j is the deuterium (j) ionization source rate, to obtain a generalized pressure diffusion equation[15]:

$$-\frac{\partial}{\partial r}\left(\frac{D_j}{T_j}\frac{\partial p_j}{\partial r}\right) + \frac{\partial}{\partial r}\left(\frac{p_j V_{r,j}^{pinch}}{T_j}\right) = S_j \quad . \tag{8}$$

In these formulations, it has been assumed that the carbon impurity pressure gradient scale length is the same as the one for the deuterium main ions. Without this assumption, there would be diffusive terms with slightly different coefficients proportional to the carbon density and temperature gradients present in Eq. (8), and a second generalized diffusion equation for the carbon density would also be required.[15]

Equation (8) will be solved numerically for the deuterium ion density, using various finite-difference approximations used with diffusion equations and employing experimental data to evaluate the various terms. We will then solve Eq. (8) by numerical integration to obtain an "exact" solution with which to compare, using the same evaluation of the various terms.

III. EXPERIMENTAL DATA

Experimental data were utilized from a DIII-D shot (#98889) that has been previously investigated (e.g., Refs. 13 and 24) in edge pedestal studies. As with any measured data, there can be both statistical (random) and/or systematic error in the variable profiles shown here. Steps have been taken to minimize both types of error in the data processing that produced the numbers used in this analysis. To minimize the first type of error, data values were taken from the same time slot between consecutive ELMs and averaged. For a detailed discussion of additional error minimization steps, the reader is directed to Refs. 24 and 25 for an overview of error mitigation steps and Ref. 26, which details an extensive error analysis for a DIII-D shot similar to 98889. We further note that the main comparison of this paper is between the results obtained with two different numerical methods, "exact" integration and solution of the generalized diffusion equation, using the same experimental data to evaluate parameters, so that any error in experimental data is of secondary importance. The shot parameters of shot 98889 utilized for this research are shown in Table I.

TABLE I

Parameters from Shot 98889, an H-Mode Discharge on DIII-D

Time range	3.75 to 4.11 s
Divertor	Lower single null
Plasma current	1.2 MA
Toroidal field	2.01 T
Major radius	1.75 m
Minor radius	0.60 m
Beam power	3.1 MW
Electron density	0.4×10^{20} m^{-3}
Poloidal field	0.22 T
Loop voltage	0.04 V/m
Triangularity δ	0.135
Elongation κ	1.75

The noncircular geometry of the plasma flux surfaces was modeled by an effective circular model, conserving flux surface area. The measured data were mapped poloidally to obtain flux-surface averaged values for comparison with calculations. The minor radius of the effective circular model is $\bar{r} = r\sqrt{0.5(1+\kappa^2)}$, which leads to an effective minor radius $\bar{a} = 0.86$ m. The circular model was used to calculate flux-surface averaged quantities at normalized radii $\rho = \bar{r}/\bar{a}$.

The experimental data used in this paper were measured just above the outboard horizontal midplane. These data were fitted at 25 points between the separatrix $\rho = 1.0$ ($\bar{r} = \bar{a} = 0.86$ m) and inside of the H-mode edge pedestal at $\rho = 0.86$ ($\bar{r} = 0.74$ m) at intervals of $\bar{r} = 0.005$ m (Ref. 27). When calculations made use of data points on a finer mesh than this, linear interpolation was used to define those additional data points.

The fitted density and temperature profiles are shown in Fig. 1. The deuterium ion temperature was obtained from the charge exchange recombination[28] (CER) spectroscopy system installed on DIII-D. Carbon toroidal and poloidal rotation velocities were also obtained using the CER system. Figure 2 shows a fit to the measured toroidal and poloidal rotation velocities for the C^{6+} impurity, along with the calculated poloidal deuterium rotation. The ion temperature and electron density profiles were measured by Thomson scattering.

The recycling neutral flux was calculated with the GTEDGE integrated modeling code[8] using a 2-D neutral

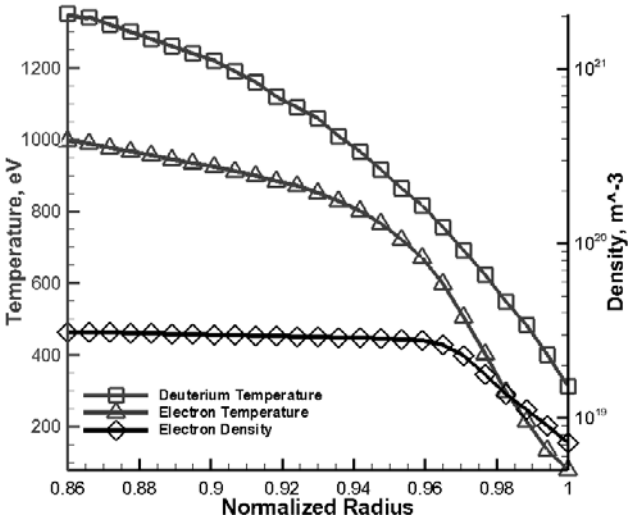

Fig. 1. DIII-D shot 98889—fitted temperature and electron density data between ELMs.

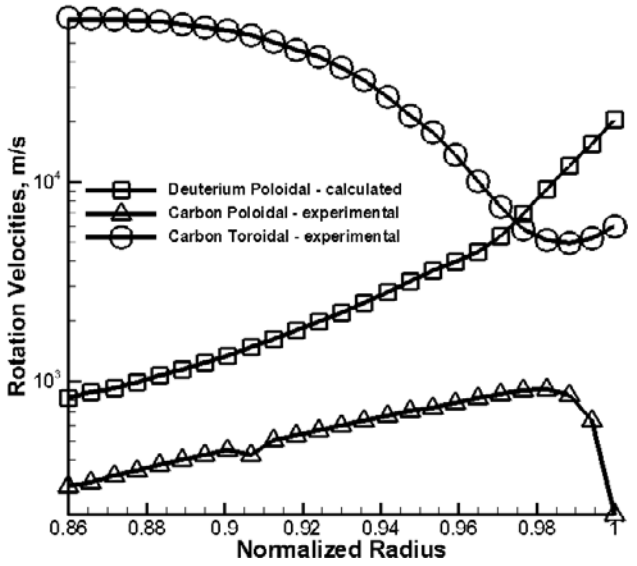

Fig. 2. DIII-D shot 98889—measured rotation velocity profiles for carbon and calculated poloidal rotation velocity profile for deuterium.

transport calculation coupled to a two-point divertor model and a core global particle and power balance.

The pinch velocity of deuterium ions was evaluated from Eq. (6) and the deuterium diffusion coefficient was evaluated from Eq. (5), using the experimental data and the calculated deuterium poloidal rotation velocity. The calculation of the deuterium poloidal rotation velocity is discussed in Ref. 24. Both quantities are shown in Fig. 3. The main contributions to the pinch velocity were from the poloidal deuterium rotation velocity and the radial electric field terms.

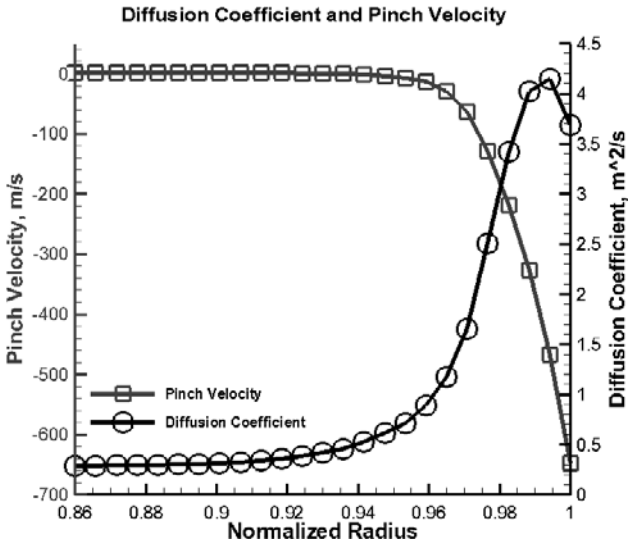

Fig. 3. DIII-D shot 98889—diffusion coefficient and pinch velocity profiles for deuterium calculated from Eqs. (5) and (6).

IV. COMPARISON OF NUMERICAL METHODS

IV.A. Numerical Algorithms for Generalized Pinch-Diffusion Equation

Numerous sophisticated and well-tested methods of solving the diffusion equation have been developed and adapted to calculate particle transport in plasmas. The major edge-transport codes, such as ONE-TWO, UEDGE, and SOLPS, have implemented such solution methods and are structured around them. Given this situation, it makes sense to investigate if the well-developed methods for solving the diffusion equation can be adapted to solve the generalized diffusion equation.

In this first investigation of the matter, the simple 1-D radial generalized pinch-diffusion equation is considered (in the slab geometry approximation). Equation (8) is integrated to solve for the density (after dividing the pressure by the experimental ion temperature), using three different numerical approximations for the pinch term as well as using different mesh spacings. Standard finite-difference approximations are used in the discretization of Eq. (8); the widely used central-difference approximation is always used with the diffusive term, and central-, backward-, and forward-difference approximations are used to evaluate the pinch term. After these approximations have been implemented, a tridiagonal matrix solution (Gauss reduction[29] or forward elimination/backward substitution) is employed to solve for the pressure at each point, and the known experimental temperatures are then used to calculate the density profiles. These density profiles are then compared to the "exact" calculated density profiles to investigate the

accuracy of the discretization approximations for the pinch term.

IV.B. "Exact" Numerical Evaluation of Density Profile

Rearranging Eq. (4) results in an equation that defines the deuterium ion pressure profile,

$$\frac{-1}{p}\frac{\partial p}{\partial r} = \frac{V_{r,j} - V_{r,j}^{pinch}}{D_j} \quad , \tag{9}$$

which may be integrated numerically to obtain the "exact" density profile when the experimental deuterium ion temperature is used to evaluate $n_j = p_j/T_j$. To carry out this calculation, experimental data are used to determine $V_{r,j}$ from Eq. (7), $V_{r,j}^{pinch}$ from Eq. (6), and D_j from Eq. (5). Then Eq. (9) is integrated numerically between mesh points j and $j + 1$ to obtain the "exact" relation for advancing the pressure solution between mesh points:

$$p_{j,i+1} = p_{j,i}\exp\!\wedge\!\left[\frac{\Delta}{2}\left(\frac{(V_{r,j,i+1}^{pinch} - V_{r,j,i+1})}{D_{j,i+1}} + \frac{(V_{r,j,i}^{pinch} - V_{r,j,i})}{D_{j,i}}\right)\right] . \tag{10}$$

This is termed the "exact" solution because it is the numerical integration of the pinch-diffusion relation. This solution is the benchmark used in this paper to compare with the finite-difference methodology solution. Here the new subscript i indicates the mesh point. This algorithm was used to advance the pressure inward from the value at the separatrix, which was taken from experiment, and the density was then calculated at each point from $n_j = p_j/T_j$. The quantity Δ is the mesh spacing.

IV.C. Data Treatment and Mesh Spacing in the Numerical Solution

The main purpose of this paper is to investigate the differences between the "exact" numerical solutions of Eq. (10) and the solutions of the conventional finite-difference approximations of the generalized diffusion equation of Eq. (8), using the same data to evaluate both. A secondary purpose is to compare both of these solutions with the independently measured density profile.

The data used for this study consist of both measured and calculated plasma properties averaged over flux surfaces at 25 points in the edge of the plasma, ranging from $\rho = 1.0$ inward with a separation of $\bar{r} = 0.005$ m between points. The widely used finite-difference approximations may be derived from Eq. (8) by making different assumptions about the data variation between mesh points.

IV.D. Discretization of the Generalized Diffusion Equation

The central-difference approximation can be derived by integrating over the interval $i - 0.5\Delta < r < i + 0.5\Delta$, treating the data as constant over this interval. The diffusion term is a perfect differential, and this integration leads to the well-known and widely used central-difference approximation. Other choices of integration interval lead to the "forward" and "backward" difference approximations to the diffusion term.

The pinch term was evaluated at point i in three different ways. In the forward-difference approximation, the pinch term was evaluated by representing the derivative at point i with the forward-difference approximation. The backward-difference approximation was implemented by representing the derivative of the pinch term at point i with the backward-difference approximation. In the central-difference approximation, the derivative of the pinch term was evaluated with the central-difference approximation.

In each case, the discretized finite-difference representation of Eq. (8) is of the form

$$(a_{i,i-1}^*)p_{i-1} + (a_{i,i}^*)p_i + (a_{i,i+1}^*)p_{i+1} = S_i^* \quad , \tag{11}$$

where the definitions of the a_{nm}^* coefficients and the source term are given by

$$a_{i,i-1}^* = \frac{-D_{j,i}}{2\Delta T_{j,i}} + \frac{-D_{j,i-1}}{2\Delta T_{j,i-1}} + \alpha \ ;$$

$$a_{i,i}^* = \frac{D_{j,i+1}}{2\Delta T_{j,i+1}} + \frac{D_{j,i}}{\Delta T_{j,i}} + \frac{D_{j,i-1}}{2\Delta T_{j,i-1}} + \beta \ ;$$

$$a_{i,i+1} = \frac{-D_{j,i+1}}{2\Delta T_{j,i+1}} + \frac{-D_{j,i}}{2\Delta T_{j,i}} + \gamma \ ;$$

$$S_j^* = S_{j,i}\Delta \ . \tag{12}$$

The α, β, and γ terms in Eq. (12) depend on the type of finite-difference approximation used for the pinch term and are displayed in Table II.

A tridiagonal Gauss reduction matrix solution[29] (forward elimination/backward substitution) can be used to solve the set of Eqs. (11) exactly. A known density separatrix boundary condition and a zero current inner boundary condition were used.

IV.E. Characteristic Length and Error of Finite-Difference Approximation

It is instructive to investigate the intrinsic accuracy of the different finite-difference algorithms by comparing them with the "exact" solution of Eq. (8) in the absence of a source.

Solving the source-free pinch-diffusion relation [Eq. (4)],

$$\frac{1}{p_j}\frac{\partial p_j}{\partial r} = \frac{V_{r,j}^{pinch}}{D_j} \quad , \tag{13}$$

TABLE II

Definitions of Terms Used in Eq. (12) Grouped by Finite-Difference Method Used with the Pinch Term

	Forward	Backward	Central
α	0	$\frac{-V_{r,j,i-1}^{pinch}}{T_{j,i-1}}$	$\frac{-V_{r,j,i-1}^{pinch}}{2T_{j,i-1}}$
β	$\frac{-V_{r,j,i}^{pinch}}{T_{j,i}}$	$\frac{V_{r,j,i}^{pinch}}{T_{j,i}}$	0
γ	$\frac{V_{r,j,i+1}^{pinch}}{T_{j,i+1}}$	0	$\frac{V_{r,j,i+1}^{pinch}}{2T_{j,i+1}}$

results in the "exact" algorithm for advancing the solution from mesh point i to $i + 1$:

$$p_{j,i+1} = p_{j,i}\, e^{\Delta V_{r,j}^{pinch}/D_j} \quad . \tag{14}$$

The characteristic length L is defined

$$L \equiv |D_j / V_{r,j}^{pinch}| \quad . \tag{15}$$

Because of the sharply increasing pinch velocity magnitude in the edge, the characteristic length sharply decreases near the separatrix, as shown in Fig. 4.

A source-free version of Eq. (11) can be compared with the "exact" solution of Eq. (13) to obtain an expression for the error associated with the various finite-difference algorithms:

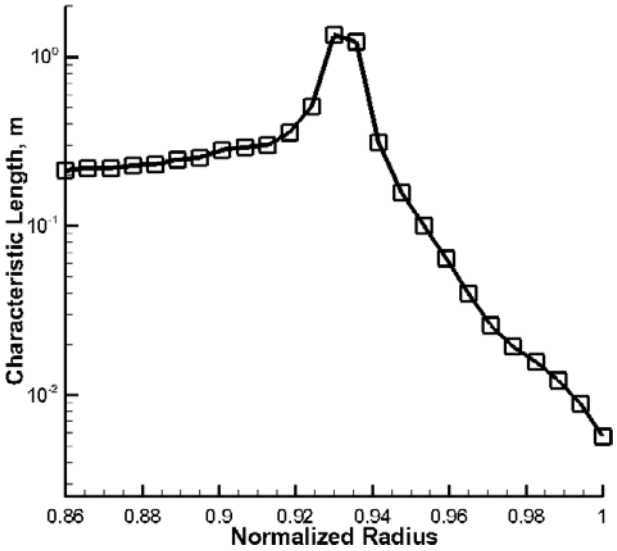

Fig. 4. DIII-D Shot 98889—deuterium characteristic length profile [of Eq. (15)] from data in Fig. 3.

$$error \cong \frac{1}{2}\left(\frac{\Delta}{L}\right)^3 \times \begin{cases} 1 - \frac{1}{3}\frac{\Delta}{L} + \ldots & \text{backward difference} \\ 1 & \text{central difference} \\ 1 + \frac{1}{3}\frac{\Delta}{L} + \ldots & \text{forward difference} \quad . \end{cases} \tag{16}$$

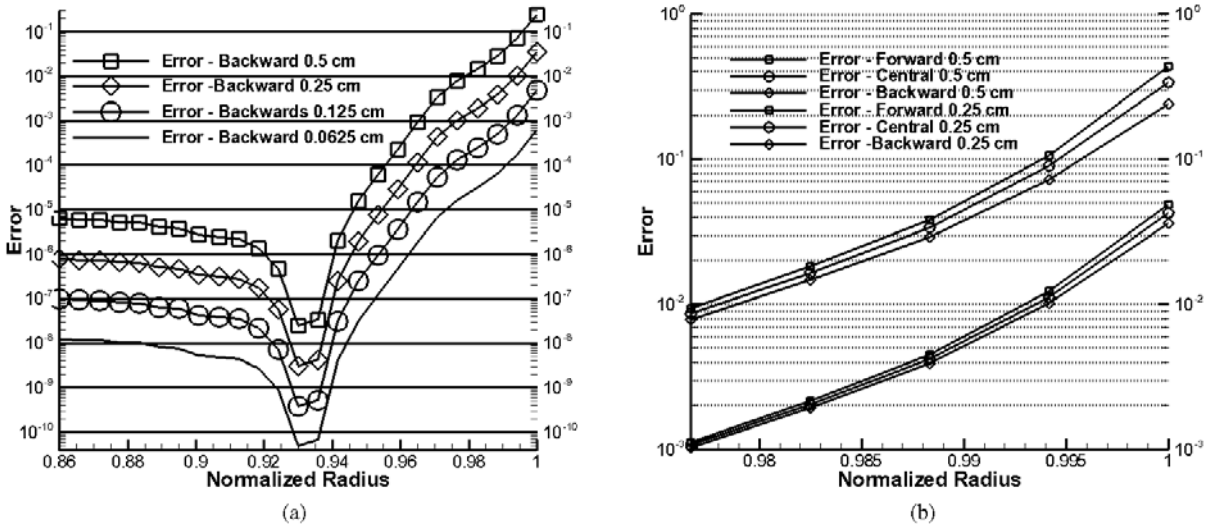

Fig. 5. DIII-D Shot 98889—(a) error of backward-difference approximation [see Eq. (11) and Table II] for various mesh spacings. (b) Enlarged variant of Fig. 5a showing the differentiation between the error profiles of the three finite-difference approximations near the separatrix. This differentiation is difficult to discern at mesh spacings smaller than 0.25 cm.

Equation (16) gives an approximation of the difference between the "exact" numerical integration of the pinch-diffusion relation and the numerical solution of the generalized diffusion equation using the finite-difference approximations. It is meant to represent error inherent in using the finite-difference approximations to solve the generalized diffusion equation rather than using the "exact" numerical integration to the pinch-diffusion relation. It is not a measure of either solution method's deviation from experimental profiles, but a measure of the deviation of the finite-difference method solution from the "exact" numerical solution.

The errors predicted by Eq. (16) are plotted in Figs. 5a and 5b for different choices of the finite-difference algorithm and mesh spacing, showing the error of the backward difference as the lowest, then the central difference, then the forward difference. The error is very sensitive to the local value of the characteristic length L, as can be seen by comparing Figs. 4 and 5a, and to the value of the mesh spacing. Clearly, a small value of Δ/L is required for precision when solving the generalized diffusion equation using the finite-difference approximations. The error is not sensitive to the finite-difference algorithm except when Δ/L approaches unity, which it does for the larger mesh spacings just inside the separatrix. This dependence is shown in detail in Fig. 5b. At smaller mesh spacings, below 0.25 cm, the differences among the finite-difference algorithm results are small, and these mesh

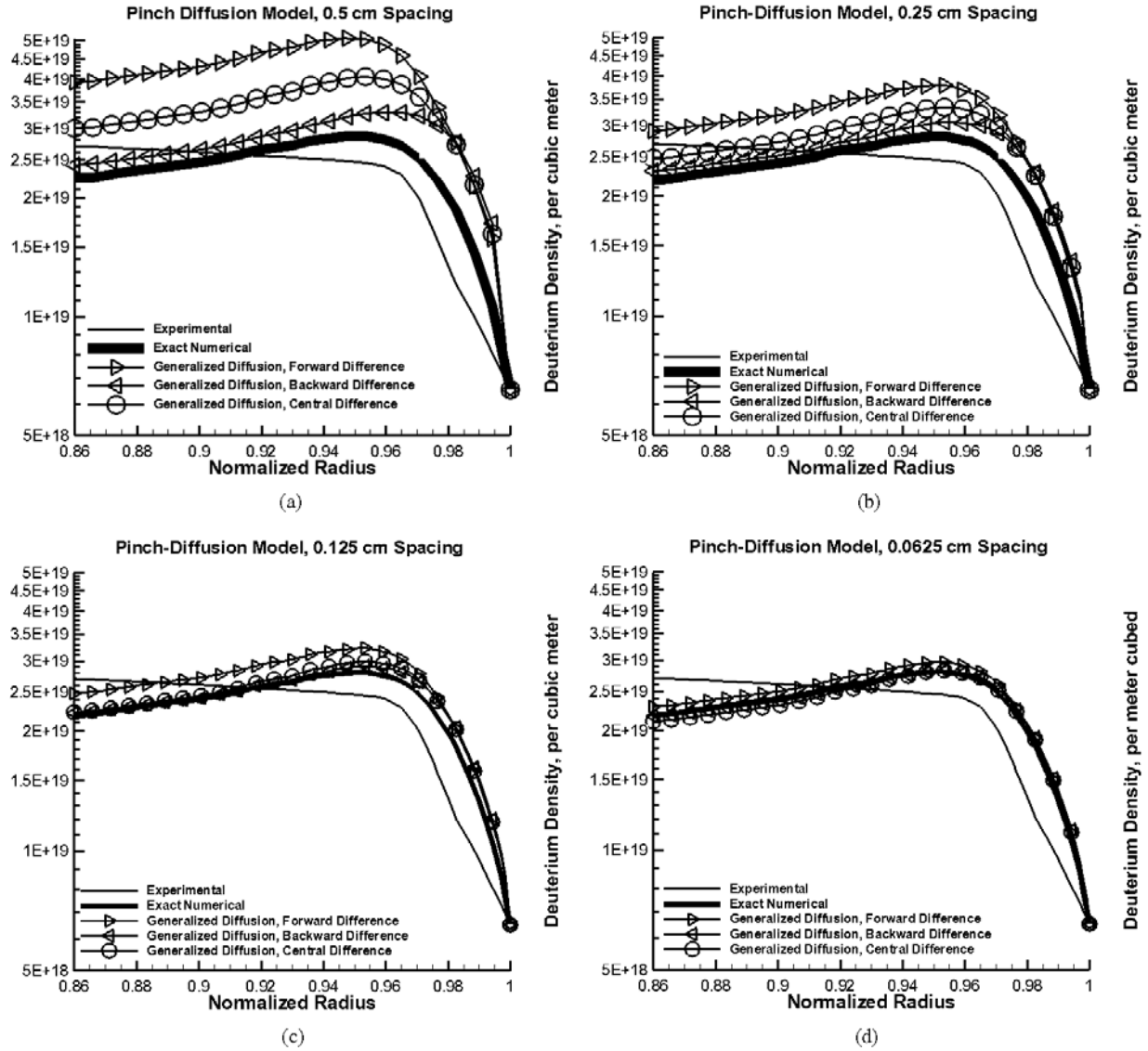

Fig. 6. DIII-D Shot 98889—results of the numerical calculation showing the solutions from the three finite-difference solution methodologies, the "exact" exponential solution, and the experimental density for reference purposes, at different mesh spacings.

spacings are not shown in Fig. 5b. The backward-difference error shown in Fig. 5a can be taken as roughly representative of the error of the central- and forward-difference algorithms for these smaller mesh spacings. The implication is that for a fixed mesh spacing Δ the error becomes larger in the edge where the pinch velocity becomes larger, so that a variable mesh with finer spacing in the edge is required to obtain a comparable accuracy at all locations.

V. COMPARISON OF NUMERICAL SOLUTIONS

The solutions obtained by solving the finite-difference generalized diffusion Eqs. (11) are compared with the "exact" numerical integration of Eq. (9) given by Eq. (10) in Fig. 6, for different choices of the mesh spacing and the finite-difference algorithm. The measured ion density is also shown in Fig. 6. It is clear that reducing the mesh spacing improves the agreement of the solution of the generalized diffusion equation with the "exact" numerical integration of Eq. (9), as would be expected from the fact that the error $\approx (\Delta/L)^3$ is reduced as the mesh spacing is reduced. This mesh spacing dependence is shown in Fig. 7. The differences between the solutions corresponding to the different finite-difference algorithms also decrease with decreasing mesh spacing, as predicted by Eq. (16). These differences in the solutions of the generalized diffusion equation relative to the "exact" solution are consistent with the error analysis displayed in Fig. 5b.

It should be noted that the generalized diffusion equations are solved with a fixed experimental boundary condition at $\rho = 1.0$ on the right and that there is a large error (up to ~50%) in the generalized diffusion solution just inside the separatrix, as shown in Fig. 5a. This error causes an overprediction of the solution just inside the separatrix, which then propagates inward even though the error in the solution propagation algorithm is much less farther inside the separatrix. This effect of the error magnitude just inside the separatrix on the solution over the entire pedestal is illustrated in Figs. 5a and 7.

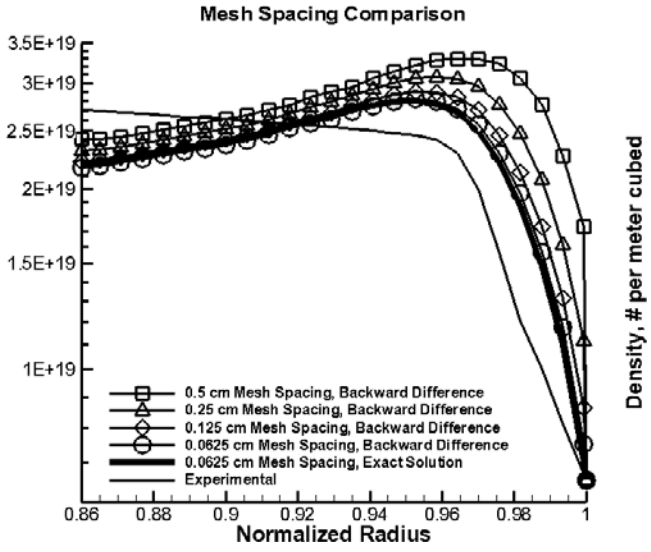

Fig. 7. Results of the numerical calculation using the backward-difference methodology, along with the "exact" exponential solution profile and the experimental profile for reference. This illustrates sensitivity of the numerical results to smaller mesh spacing.

In this work, an investigation is carried out into the use of finite-difference methodology to solve the generalized diffusion equation. The difference between the solution of the generalized diffusion equation using finite-difference methodology and the solution to the pinch-diffusion relation using "exact" exponential methodology is the error inherent in the finite-difference numerical methodology. Aside from the error inherent in non-"exact" solution methodology, there are inaccuracies in diffusion theory, assumptions made for the model, data measurement and processing error, etc. This additional error is what differentiates even the "exact" solution and converged finite-difference methodology solutions from the experimental values. However, this deviation is not the focus of this paper, and the experimental ion density profiles (electron densities measured by Thomson scattering and corrected for the measured carbon impurity density) are shown along with the results only to serve as a familiar reference.

These differences between the "exact" numerical solution and the experimental density must be attributed to remaining inaccuracies in the evaluation of the experimental values for the parameters used to solve Eq. (9) (most likely the determination of deuterium poloidal velocity contributes a large part of this discrepancy) and to the use of a slab model for the calculation. The assumption that the carbon and deuterium logarithmic pressure gradients are the same, made in deriving Eq. (9), is not thought to contribute significantly to the error shown in Fig. 6.

VI. SUMMARY AND CONCLUSIONS

The large pinch velocity in the plasma edge of H-mode tokamak plasmas requires that a pinch-diffusion relation for the particle flux be used in order to satisfy momentum balance, which leads to a generalized diffusion theory with a pinch term. The ability to represent and solve this generalized diffusion equation, using the same type of finite-difference approximations and solution algorithms used with the standard diffusion theory finite-difference algorithms employed in major plasma edge codes, has been investigated numerically. The error in the standard finite-difference representation of the generalized diffusion equation was shown to be $\approx (\Delta/L)^3$, where Δ is the mesh spacing and $L = |D_j/V_{r,j}^{pinch}|$ is the characteristic length. This error was shown to be quite large just inside the separatrix, where L becomes small because

the pinch velocity becomes large, which can cause an error in the density solution that propagates into the pedestal region unless the mesh spacing is sufficiently small just inside the separatrix. The implication is that a variable mesh spacing should be used for solving the generalized diffusion equation in the plasma edge, with finely spaced mesh just inside the separatrix where the pinch velocity is large. Making use of such a variable mesh spacing, it should be possible to extend existing diffusion theory codes to solve the momentum balance equation to correctly represent particle transport in the edge pedestal so as to satisfy momentum balance.

ACKNOWLEDGMENTS

The authors would like to thank R. J. Groebner for providing the fits to the DIII-D experimental data used in this analysis and express their appreciation to the DIII-D team for the use of the data. This work was supported by the U.S. Department of Energy grant DE-FG02-00-ER54538 with the Georgia Tech Research Corporation.

REFERENCES

1. C. F. MAGGI, *Nucl. Fusion*, **50**, 066001 (2010).

2. T. H. OSBORNE et al., *Proc. 24th European Conf. Controlled Fusion and Plasma Physics*, Berchtesgaden, Germany, June 9–13, 1997, Vol. 21A, Part III, p. 1101, European Physical Society (1997).

3. M. GREENWALD et al., *Nucl. Fusion*, **37**, 793 (1997).

4. W. SUTTROP et al., *Plasma Phys. Control. Fusion*, **39**, 2051 (1997).

5. M. KOTSCHENREUTHER et al., *Proc. 16th Int. Conf. Fusion Energy*, Montreal, Canada, October 7–11, 1996, Vol. 2, p. 371, International Atomic Energy Agency (1996).

6. J. E. KINSEY, G. BATEMAN, T. ONJUN, A. H. KRITZ, A. PANKIN, G. M. STAEBLER, and R. E. WALTZ, *Nucl. Fusion*, **43**, 1845 (2003).

7. H. E. ST. JOHN, T. S. TAYLOR, Y. R. LIN-LIU, and A. D. TURNBULL, *Proc. 15th Int. Conf. Plasma Physics and Controlled Nuclear Fusion Research*, Seville, Spain, September 26–October 1, 1994, Vol. 3, p. 603, International Atomic Energy Agency (1995).

8. W. M. STACEY, *Phys. Plasmas*, **5**, 1015 (1998); see also W. M. STACEY, *Phys. Plasmas*, **8**, 3673 (2001); see also W. M. STACEY, *Nucl. Fusion*, **40**, 965 (2000).

9. G. V. PEREVERZEV and P. N. YUSHMANOV, "ASTRA: Automated System for Transport Analysis," IPP 5/98, Max-Planck Institut fur Plasmaphysik (Feb. 2002).

10. R. SCHEIDER et al., *Contrib. Plasma Phys.*, **46**, 3 (2006).

11. T. D. ROGNLIEN, M. E. RENSINK, and G. R. SMITH, "User Manual for the UEDG Edge-Plasma Transport Code," UCRL-ID-137121, Lawrence Livermore National Laboratory (Feb. 23, 2007).

12. T. D. ROGNLIEN and M. E. RENSINK, *Fusion Eng. Des.*, **60**, 497 (2002).

13. J. D. CALLEN et al., *Nucl. Fusion*, **50**, 064004 (2010).

14. W. M. STACEY, *Phys. Plasmas*, **11**, 5487 (2004).

15. W. M. STACEY, *Contrib. Plasma Phys.*, **48**, 94 (2008).

16. L. A. ARTSIMOVICH, *Plasma Phys. Control. Nucl. Fusion Res.*, **2**, 595 (1966).

17. E. P. GORBUNOV, *Plasma Phys. Control. Nucl. Fusion Res.*, **2**, 629 (1966).

18. B. COPPI and N. SHARKEY, *Nucl. Fusion*, **21**, 1363 (1981).

19. M. E. RENSINK, S. L. ALLEN, A. H. FUTCH, D. N. HILL, G. D. PORTER, and M. A. MAHDAVI, *Phys. Fluids B*, **5**, 2165 (1993).

20. W. M. STACEY and R. J. GROEBNER, *Phys. Plasmas*, **14**, 012501 (2007).

21. R. J. GROEBNER, T. H. OSBORNE, A. W. LEONARD, and M. E. FENSTERMACHER, *Nucl. Fusion*, **49**, 045013 (2009).

22. R. J. GROEBNER et al., *Nucl. Fusion*, **49**, 085037 (2009).

23. A. KALLENBACH et al., *Plasma Phys. Control. Fusion*, **46**, 431 (2004).

24. W. M. STACEY and R. J. GROEBNER, *Nucl. Fusion*, **51**, 063024 (2011).

25. W. M. STACEY and R. J. GROEBNER, *Phys. Plasmas*, **15**, 012503 (2008).

26. R. J. GROEBNER et al., *Nucl. Fusion*, **50**, 064002 (2010).

27. R. J. GROEBNER, General Atomics, Personal Communication (2010).

28. P. GOHIL, K. H. BURRELL, R. J. GROEBNER, J. KIM, W. C. MARTIN, E. L. McKEE, and R. P. SERAYDARIAN, *Proc. 14th IEEE/NPSS Symp. on Fusion Engineering*, San Diego, California, September 30–October 3, 1991, Vol. 2, p. 1199, IEEE (1992).

29. W. H. PRESS, B. P. FLANNERY, S. A. TEUKOLSKY, and W. T. VETTERLING, *Numerical Recipes in Fortran: The Art of Scientific Computing*, pp. 29–31, Cambridge University Press, New York (1986).